Optimization of the End Cells in SRF Cavities

Jonathan Luk
Universtity of California, San Diego, La Jolla, CA 92093
(Dated: August 12, 2005)

The shape of the end cells of the RF superconducting cavities was optimized by numerical calculations in order to maximize the acceleration. A study has also been done to investigate the acceleration in the end cells with geometry that would possibly extract higher order modes.

I. INTRODUCTION

The work on increasing the accelerating gradient E_{acc} in RF superconducting niobium resonators has not terminated. An accelerating gradient of 46 MV/m (CW) has been achieved at Cornell in 2004 [1][1]. Here, E_{acc} is defined as $E_{acc} = \frac{\int_0^L E\,dx}{L}$, which is the average electric field in a cell with length L, where $E_z(z)cos(\omega t) = E_z(z)cos(\frac{2\pi z}{\lambda})$ has taken into account the change of the field in time. One of the possibilities to increase E_{acc} is the optimization of the cavity shape [2].

The limit of the accelerating gradient is imposed by $\frac{H_{pk}}{E_{acc}}$, a ratio that is fixed by geometry, because H_{pk} is bounded above by the critical magnetic field $H_{crit,RF}$, above which superconductivity breaks down [1, 3]. $\frac{E_{pk}}{E_{acc}}$ may also impose a limit because E_{pk} being too high would cause the danger of field emission [3]. However, since the limit of E_{pk} can be raised by better cleanliness and high power processing while H_{pk} is a hard limit, it is justifiable to reduce H_{pk} by sacrificing E_{pk} up to a certain bound.

Previous optimization has been done for the inner cells in SRF cavities to reduce $\frac{H_{pk}}{E_{acc}}$ for given values of $\frac{E_{pk}}{E_{acc}}$ [2, 4]. However, there is yet to be a systematic description of the optimization of the end cells in SRF cavities.

Unlike the optimization of the inner cells, it is more reasonable to consider maximizing V_{acc} with the optimization of the end cells. This is because the electric field, in theory, extends to infinity in the tube (but with converging integral) and the definition of E_{acc} becomes dependent on the tube length. The physically significant figure is the value of acceleration $V_{acc} = \int_0^{+\infty} E\,dx$, and this is the value that we will maximize.

In order to evaluate the improvement by the optimization, we compare the ratios $\frac{H_{pk}}{V_{acc}}$ and $\frac{E_{pk}}{V_{acc}}$ with that of TESLA. For inner TESLA cells, $\frac{E_{pk}}{E_{acc}} = 2.0$ and $\frac{H_{pk}}{E_{acc}} = 42$ Oe/(MV/m) [5]. We thus define $e = \frac{E_{pk}L}{2V_{acc}}$ and $h = \frac{H_{pk}L}{42V_{acc}}$ with $L = 57.6524$ mm (a quarter of wavelength, $\frac{\lambda}{4}$, for frequency of 1300 Hz) being the length of the inner cell so that comparison can be made between inner and end cells. For TESLA cells, $e = h = 1$. Since we can make sacrifice for e, the optimization of the inner cells has been previously done by letting $e = e_0 = 1.2$ and reducing h. Suppose the minimal h achieved for the inner cells was h_0, which is different for different R_{bp}. (For $R_{bp} = 35$ mm, for example, $h_0 = 0.8996$, i.e., 10% less than the case of TESLA.) We would then like to minimize $max\{\frac{e}{1.2}, \frac{h}{h_0}\}$ for the end cells. The minima

[1] Recents tests (July, 2005) of another reentrant Cornell cavity at KEK (Japan) confirmed this experiment with the result of 47 MV/m (K. Saito, private communication).

must be obtained such that E_{pk} and H_{pk} are attained at the inner end. In this case, we expect the fields in the inner half of the end cell to be identical to that in the inner cells and $max\{\frac{e}{1.2}, \frac{h}{h_0}\} = \frac{e}{1.2} = \frac{h}{h_0}$.

A previous study has shown that smaller iris radii would further increase the accelerating gradient [6]. This is therefore an incentive for studying the effect of different iris radii on the fields in the end cells. We also studied the possibility of different beam pipe radii because broader beam pipe can help to extract higher order modes.

II. THE CODE FOR OPTIMIZATION

The SLANS code [7] is used for this study. It is a code designed for numerical calculations of the fields in the monopole modes of axisymmetric cavities. It uses a finite element method of calculation with a mesh of quadrilateral biquadratic elements [8]. In a study comparing different codes for calculating the fields in a spherical cavity, SLANS was shown to have better performance [9].

For the optimization of the end cells, a special envelop code TeslaGeom_end was written by Dmitry Myakishev, the author of SLANS. This envelop code automates the tuning the frequency of a cell by changing its length. It also makes it possible to calculate a batch of cells with different parameters: half-axis A, B and a (Fig. 1). Another version of this envelop code (TeslaGeom) was used earlier for the optimization of the inner cells [6].

III. THE GEOMETRY FOR OPTIMIZATION

For this optimization, we employ the same construction of the profile line as that of the inner cells [4]. This is constructed as two elliptic arcs (Fig. 1). It has been shown that this shape achieves a better accelerating gradient than that of the "circular arc - straight segment - elliptic arc" profile line as in TESLA [2].

We only optimize the outer half of the end cell because for the other half we chose a geometry identical to that of the inner cells, which has already been optimized. For the geometry in Fig. 1, we have three independent variables to optimize, namely, A, B and a. The other axis of the ellipse, b, is fixed by geometry since the two ellipses must have a common tangent at the contact point. R_{eq} is fixed by the optimization of the inner cell. L is chosen by tuning to the correct frequency. (This is different from the optimization of the inner cells where L was fixed to be $\frac{\lambda}{4}$ and the frequency is tuned by changing R_{eq}.) The frequency that is used is 1300 MHz, but the optimization is valid for any frequency: one needs only to scale all the dimensions.

IV. LENGTH OF THE BEAM PIPE

The integration $V_{acc} = \int_0^{+\infty} E\,dx$ as described above can be approximated by numerical calculations with an appropriate choice of the upper integration limit. It has to be a sufficiently large yet finite number so that the error is sufficiently small. It is also important that the integration limit is not too large for otherwise error will arise from the large mesh size.

We aim at an accuracy of four decimal places in e and h. Since e and h varies from 0.8 to 1.3, they can be taken, for simplicity, to be 1 and thus the absolute error can be taken as

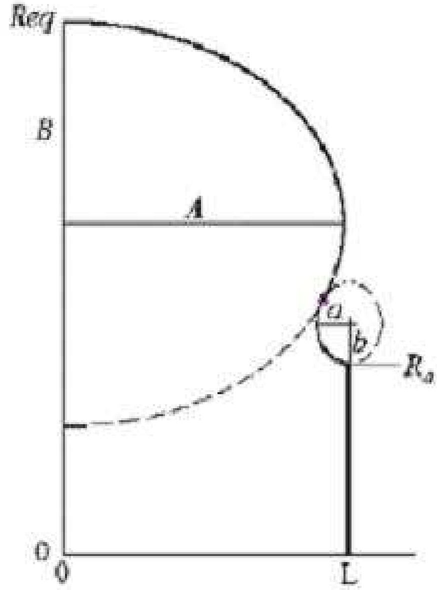

FIG. 1: Geometry for Calculation

the relative error. This, in turn, by the formula of e and h, is given by the relative error of V_{acc}, i.e., $\frac{\Delta V_{acc}}{V_{acc}}$.

The electric field of the fundamental mode in the beam pipe follows an exponential decay $e^{-\alpha z}$, where $\alpha = \frac{2\pi\sqrt{f_c^2-f^2}}{c}$, with f_c, f and c being the cutoff frequency, frequency of the wave and the speed of light respectively. The calculation of f_c is described in the section of Higher Order Modes. Supposing the cavity extends from 0 to L_c and the pipe extends from L_c to $L_c + L_t$ (Fig. 2), then the relative error of V_{acc} is given by

$$\frac{\Delta V_{acc}}{V_{acc}} = \frac{\int_{L_c}^{+\infty} E\,dz}{\int_0^{+\infty} E\,dz}\frac{\int_{L_c+L_t}^{+\infty} E\,dz}{\int_{L_c}^{+\infty} E\,dz} \approx \frac{\int_{L_c}^{L_c+L_t} E\,dz}{\int_0^{L_c+L_t} E\,dz}e^{-\alpha L_t}. \tag{1}$$

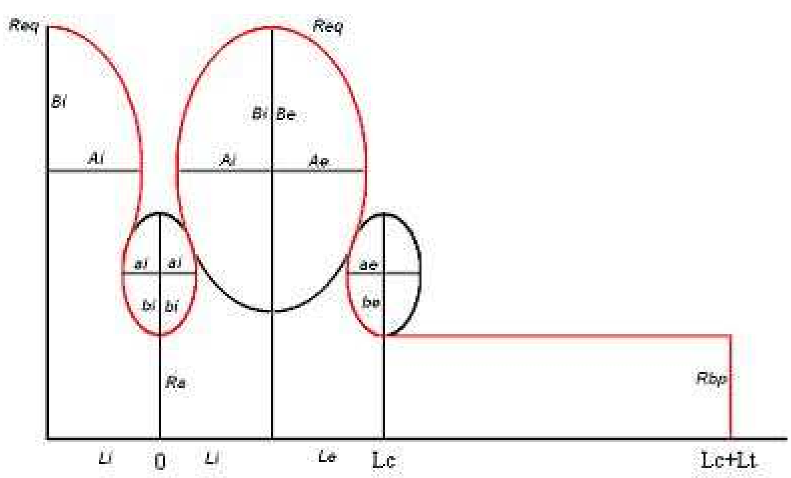

FIG. 2: The Dimensions of End Cells with $R_a = R_{bp}$

To carry out the approximation, we use the case of $R_{bp} = 35$ mm. The first fraction is calculated numerically to be 0.054. Previous calculations were done with $L_t = 3R_{bp}$. With this choice, the relative error was 5×10^{-4}. In order to reduce the error, we increased L to $4R_{bp}$ and the relative error became 10^{-4}. Therefore, the error in e and h was also 10^{-4}, as desired.

V. RESULTS

The optimization, with the method mentioned above, has been done for end cells with $R_a = R_{bp} = 30$ mm, 32.5 mm, 35 mm (Fig. 2). The optimized geometric parameters of the outer half of the end cells are presented in Table 1. As mentioned above, the parameters of the inner half of the end cells are taken as that of the optimized inner cells. In Table 1, the accelerating voltages of the optimized end cells are compared to that of the optimized inner cells. It is shown that the end cells, after optimization, have larger acceleration than the inner cells. The difference is more significant for smaller R_{bp} (Fig. 3).

TABLE I: Dimensions (in mm) of the optimized end cells and comparison of V in end cells and inner cells

Rbp	A	B	a	b	R_{eq}	L_e	$\frac{V_{end}}{V_{inner}}$
30.0	55.56	43.13	4.11	7.25	97.374	56.411	1.0063
32.5	54.95	42.91	4.30	7.48	98.000	56.712	1.0054
35.0	53.53	42.79	4.59	7.75	98.710	56.240	1.0041

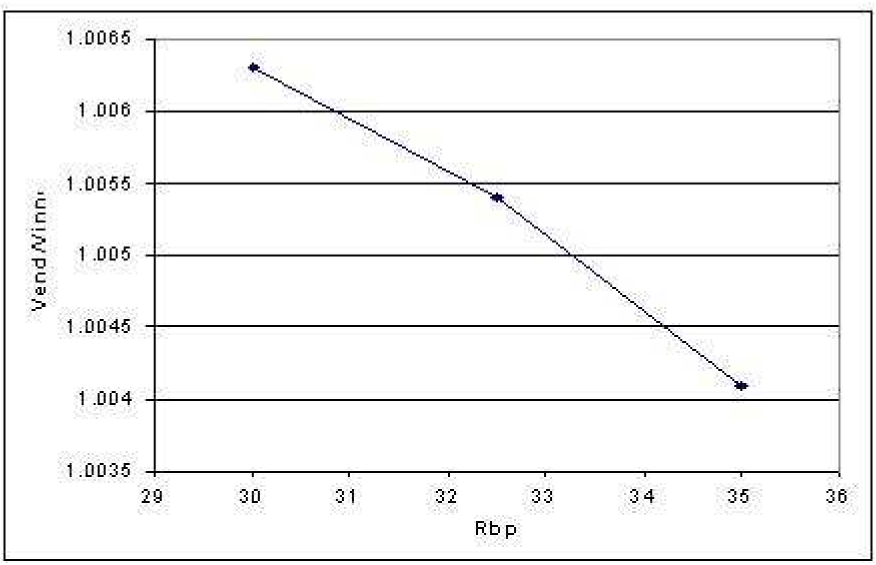

FIG. 3: The dependence of $\frac{V_{end}}{V_{inner}}$ on R_{bp}

In general, after the optimization, the "corner" between the end cell and the beam pipe becomes sharper. After the optimization, E_{pk} is attained at both ends of the end cells, i.e., the two local peaks are equal. Fig. 4 illustrates this by showing a comparison between the electric field along the profile line before and after optimization for $R_{bp} = 35$ mm.

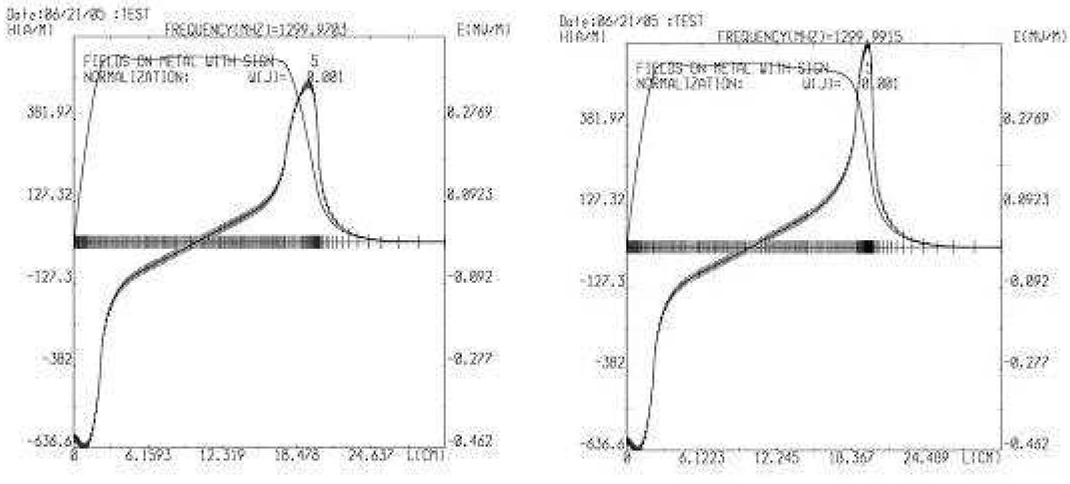

FIG. 4: Fields along profile line of the end cell before (left) and after (right) optimization

VI. RESULTS FOR SINGLE-CELL CAVITY

The optimized results for the ends cells can also be used to construct single-cell cavity (Fig. 5) to carry out an experiment on the accelerating gradient. The goal is to construct a single-cell cavity that has an accelerating gradient higher than that of the cavity which achieved a world record accelerating gradient [1].

The optimized values of both the inner cells of multi-cell cavities and single-cell cavities are presented in Table 2. The dimensions used for the single-cell cavity were the same as that in Table 1. The fields in each cell are plotted (Fig. 6). It should be noted that the fields in the end cells consist of two parts: for $R_{bp} = 30$ mm, 32.5 mm, 35 mm, the left parts are identical to the left halves of the graphs (a), (c) and (e) respectively and the right parts are identical to the right halves of the graphs (b), (d) and (f) respectively.

Table 3 shows the values of e and h for the single-cell cavity constructed with the geometric parameters of the optimized end cells. It is expected that the single-cell cavity of $R_{bp} = 30$ mm, 32.5 mm, 35 mm would show improvements of 0.63%, 0.55% and 0.41% respectively from the optimized end cells as in Table 1, i.e., improvements of 1.3%, 1.1% and 0.82% respectively from the inner cells. This is because the improvement obtained by replacing an inner half cell by an end half cell should be the same. This expectation is reached within error.

VII. HIGHER ORDER MODES

It is another goal of the optimization of the shape of the end cell to extract higher order modes (HOM) in the cavities. The HOMs include the dipole and quadrupole modes and they both have a transverse component of electric field, which will distort the beam. These HOMs

TABLE II: The dimensions (in mm) of multi-cell and single-cell cavities

	Inner cells of Multi-cell Cavity					Single-cell (using end half of end cells					
R_{bp}	A	B	a	b	L	A	B	a	b	L	R_{eq}
30	54.00	38.95	7.61	10.48	57.6524	55.56	43.13	4.11	7.25	56.411	97.374
32.5	52.84	37.53	8.29	11.24	57.6524	54.95	42.91	4.30	7.48	56.712	98.100
35	51.56	36.22	9.16	11.92	57.6524	53.53	42.79	4.59	7.75	56.240	98.710

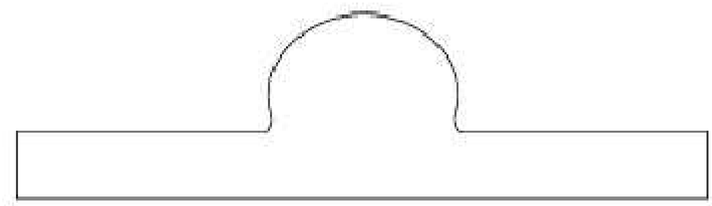

FIG. 5: Shape of single-cell cavity

can be got rid of if the beam pipe radius (R_{bp}) is chosen appropriately so that the frequencies of the HOMs are higher than the cutoff frequency of the beam pipe and consequently the HOMs will propagate out of the cavities.

The cutoff frequencies of the TE_{11} mode in the beam pipe with various R_{bp} are shown in Table 4. They are calculated by $f = \frac{t'_{11}}{2\pi R\sqrt{\mu_0\epsilon_0}}$, where $t'_{11} = 1.84118$ is the first root of derivative of the Bessel function J_1. The frequencies of the fundamental and higher order modes in the cavity are shown in the dispersion curves (Fig. 7). The dispersion curves show the phase dependence of the frequencies of each mode in an $R_{bp} = 35$ mm cavity. They are found by calculating the eigenmodes inside a 9-cell cavity with the optimized cell, i.e., the (different) optimized values of the parameters of the inner and end cells are used.

In Table 4, we also calculate the required $R_{bp}(= 55.82$ mm), above which the cutoff frequency will be lower than the frequencies of the HOMs. It should be noted that even so the problem of HOMs is not totally eliminated because some HOMs can transform so that they are not propagated out of the tube. Moreover, by increasing R_{bp} we have to make two sacrifices. First, the attenuation of the fundamental mode of the cavity will be slower. Second, as we will show in the next section, the acceleration will be lower.

TABLE III: e and h values for the single-cell cavities

R_{bp}	e	h	h_0	$\frac{e}{e_0}$	$\frac{h}{h_0}$	$\frac{v_{single}}{V_{end}}$	
30	1.1869	0.8166	1.1999	0.8333	0.9892	0.9800	1.0110
32.5	1.1890	0.8477	1.2000	0.8656	0.9908	0.9793	1.0093
35	1.1900	0.8816	1.2000	0.8996	0.9917	0.9799	1.0084

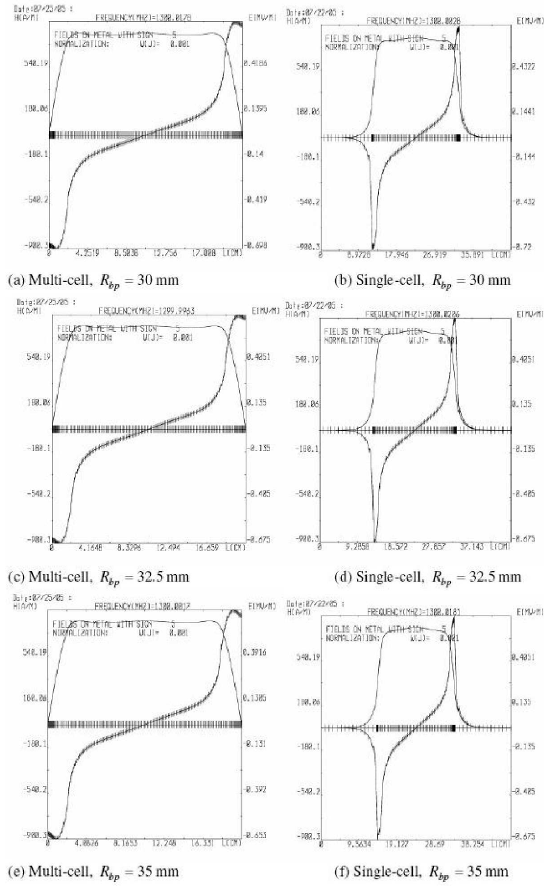

(a) Multi-cell, $R_{bp} = 30$ mm (b) Single-cell, $R_{bp} = 30$ mm
(c) Multi-cell, $R_{bp} = 32.5$ mm (d) Single-cell, $R_{bp} = 32.5$ mm
(e) Multi-cell, $R_{bp} = 35$ mm (f) Single-cell, $R_{bp} = 35$ mm

FIG. 6: Fields along the profile lines of inner cells of multi-cell cavities and single-cell cavities

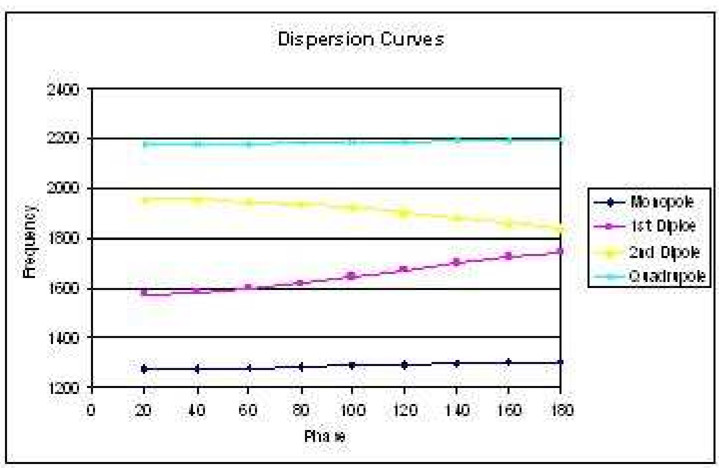

FIG. 7: Dispersion curves for $R_{bp} = 35$ mm

VIII. OPTIMIZATION WITH LARGER BEAM PIPE RADIUS

In order to reduce HOMs, we attempt to optimize two geometries with larger R_{bp}. The first geometry is shown in Fig. 8. R_{bp} is changed to be different from R_a and we investigate

TABLE IV: Cutoff frequencies of TE_{11} mode for different R_{bp}

R_{bp} /mm	f_{cutoff} /MHz
35	2509.973
40	2196.226
45	1952.201
50	1756.981
55	1597.256
55.82	1573.816
60	1464.151

its impact on V_{acc}.

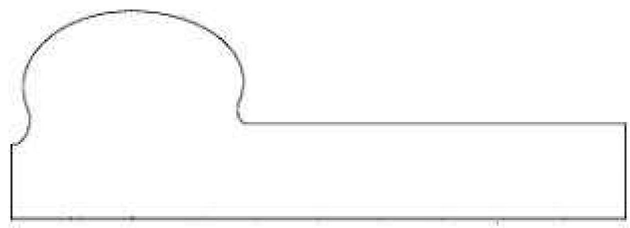

FIG. 8: The shape with $R_a < R_{bp}$

The results for $R_a = 30$ mm and $R_a = 35$ mm are shown in Fig. 9. It is shown that as we increase R_{bp} to combat HOMs, we sacrifice V_{acc}. This trade-off is more significant for $R_a = 30$ mm, where $\frac{V_{end}}{V_{inner}}$ decreases more rapidly. In fact, for the $R_{bp} = 30$ mm case, it is impossible for E_{pk} and H_{pk} to be attained at the inner half of the end cell.

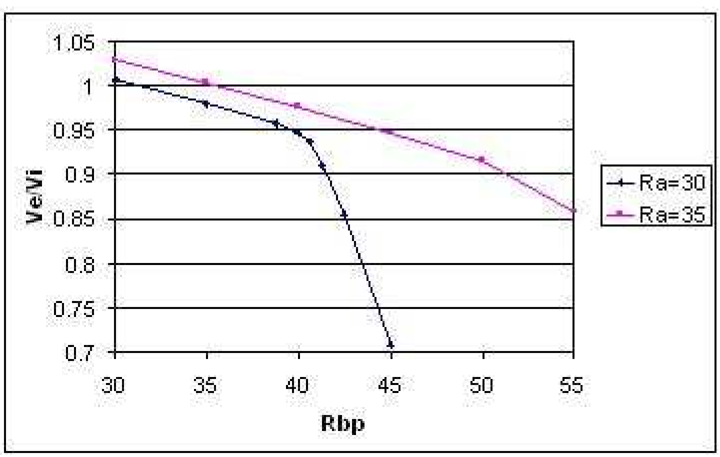

FIG. 9: $\frac{V_{end}}{V_{inner}}$ for various R_a and R_{bp} (Units in mm)

Another geometry that has been optimized is shown in Fig. 10. It should be noted that the half-cell of the inner cavity is shown for clarity but was not used in the geometry for calculations. A_i, B_i and a_i are chosen as the optimized values of the inner cells and A_e,

B_e and a_e are to be optimized as above. Before the optimization, a_t, b_t, and c are chosen arbitrarily. R_{bp} was chosen to be larger than R_{ae} so that the HOMs can be allowed to propagate out without much sacrifice in V_{acc}. The same technique was used with the one-cell KEK cavity and the two-cell cavity of the ERL injector that is under development at Cornell University. We hope to generalize this technique to multi-cell cavities.

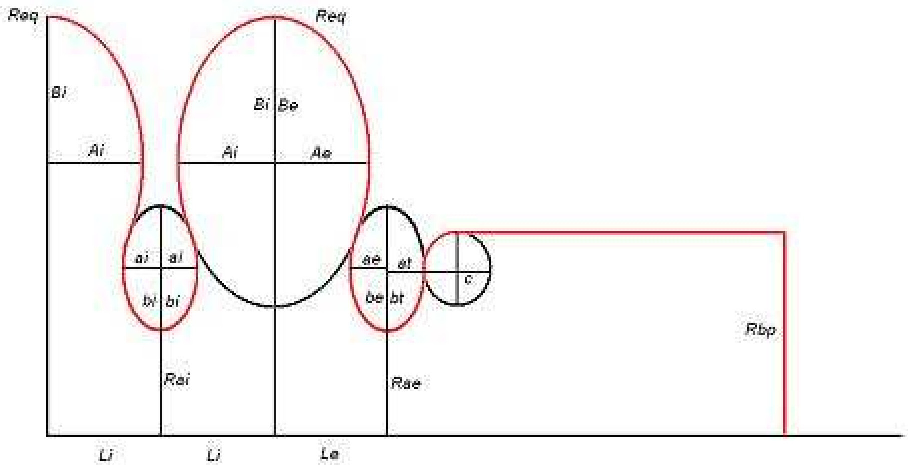

FIG. 10: Shape with different R_{ae} and R_{bp}

We optimized the cavity with $R_{ai} = 35$ mm. We set $a_t = 9.28$ mm, $b_t = 12$ mm and $c = 3$ mm (and thus $R_{bp} = 50$ mm). This initial choice of a_t and b_t is based on the curvature of ellipse in the optimized inner cell. With this choice of a_t, b_t and c, we obtained an optimized value of $\frac{V_{end}}{V_{inner}} = 0.9875$, which is nearly 8% better than the value obtained for the $R_{bp} = 50$ mm case for the above geometry.

The dependence of the optimization on a_t, b_t and c is also studied. We vary these parameters while fixing other parameters as above, including the previously optimized parameters A_e, B_e and a_e for the end cell. b_t and c are studied together in order to keep R_{bp} constant. It was shown that $max\{\frac{e}{1.2}, \frac{h}{h_0}\}$ increases with increasing b_t (Fig. 11).

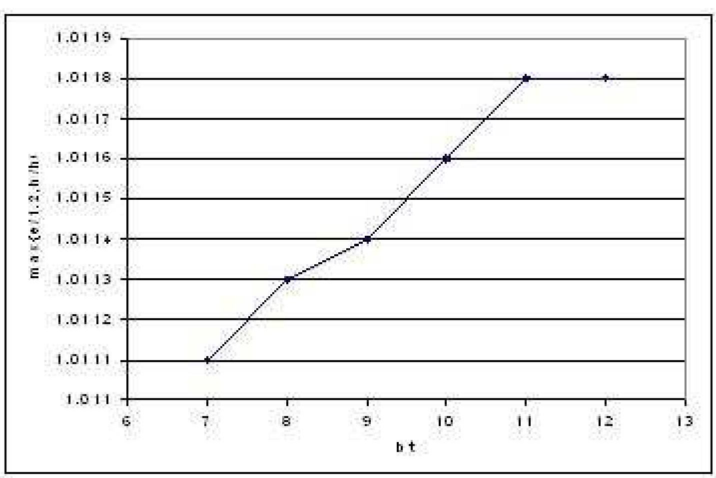

FIG. 11: The dependence of $max\{\frac{e}{1.2}, \frac{h}{h_0}\}$ on b_t in mm

In order to minimize e and h, we choose $b_t = 7$ as we study a_t. a_t is varied from 4.53 mm to 60 mm and it is shown that $max\{\frac{e}{1.2}, \frac{h}{h_0}\}$ decreases (Fig. 12), i.e., V_{acc} increases in the end cell. The decrease levels off at $a_t = 50$ mm. We then optimize this geometry with $a_t = 50$ mm, $b_t = 7$ mm and $c = 6$ mm. For this geometry, $\frac{V_{end}}{V_{inner}}$ is optimized to be 1.0026, a value that is larger than that of $a_t = 9.28$ mm but smaller than that in Table 1. It is apparent that as $a \to +\infty$, this geometry tends to the one in Fig. 2 and $\frac{V_{end}}{V_{inner}}$ increases asymptotically to 1.0041, the value in Table 1.

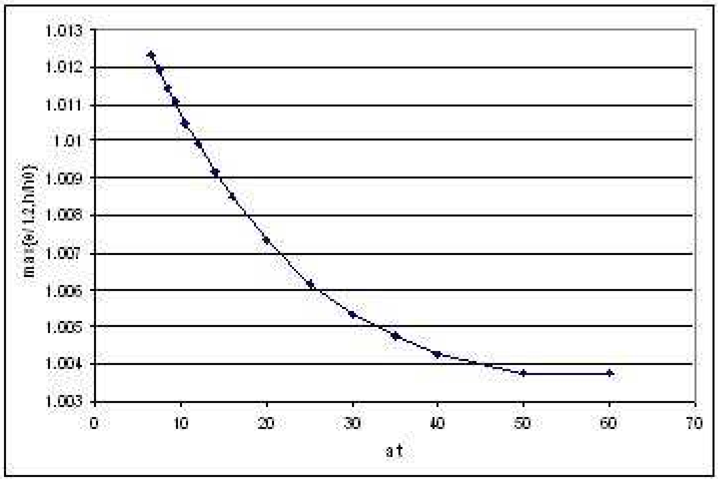

FIG. 12: The dependence of $max\{\frac{e}{1.2}, \frac{h}{h_0}\}$ on a_t in mm

IX. CONCLUSION

The end cells can be optimized to obtain V_{acc} better than that of the inner cells. Although this improvement is small (about 0.5%), this study nevertheless provides a systematic discussion of the possible improvement that can be given by the optimization of the shapes of the end cells.

The possibility of combating Higher Order Modes by increasing the beam pipe radius is also studied. The final shape has to depend on the trade-off between the reduction of Higher Order Modes and the increase in accelerating gradient. This, in turn, will depend on further study on Higher Order Modes as the beam pipe radius is increased.

X. ACKNOWLEDGMENTS

The author would like to thank his mentor, Dr. Valery Shemelin of Cornell University, for his patient guidance and helpful advice. The author would also like to thank Dr. Rich Galik for organizing the REU Program. This work was supported by National Science Foundation

REU grant PHY-0243687 and research co-operative agreement PHY-9809799.

[1] R. L. Geng, H. Padamsee, A. Seaman, V. D. Shemelin. World Record Accelerating Gradient Achieved in a Superconducting Niobium RF Cavity. PAC 2005, Knoxville, TN, May 2005.

[2] V. Shemelin, H. Padamsee. The Optimal Shape of Cells of a Superconducting Accelerating Section. Cornell University LNS Report SRF 0201128-01; 2002; TESLA Report 2002-1.

[3] H. Padamsee, J. Knobloch, T. Hays. RF Superconductivity for Accelerators. John Wiley & Sons, Inc., 1998.

[4] V. Shemelin, H. Padamsee, R. L. Geng. Optimal Cells for TESLA Accelerating Structure. Nucl. Instr. and Meth. A496 (2003) 1-7.

[5] D. A. Edwards (ed.). TESLA Test Facility Linac-Design Report. DESY Print, March 1995, TESLA 95-01.

[6] V. Shemelin. Optimized Shape of Cavity Cells for Apertures Smaller than in TESLA. PAC 2005, Knoxville, TN, May 2005.

[7] D. G. Myakishev, V. P. Yakovlev. The New Possibilities of SuperLANS Code for Evaluation of Axisymmetric Cavities, 1995 Particle Accelerator Conference and International Conference on High-Energy Accelerators. May 1-5, 1995, Texas, pp. 2348-2350.

[8] R. Paryl. SUPERLANS Companion for PC. Cornell University SRF/D 990607-01.

[9] S. Belomestnykh. Spherical Cavity: Analytical Formulas. Comparison of Computer Codes. Cornell University LNS Report SRF 941208-13, 1994.